Earth and Planetary Science Letters 345-348 (2012) 212–220

Contents lists available at SciVerse ScienceDirect

Earth and Planetary Science Letters

journal homepage: www.elsevier.com/locate/epsl

Letters

The benefit of hindsight in observational science: Retrospective seismological observations

Andrew Curtis [a,*], Yannik Behr [b,c], Elizabeth Entwistle [a], Erica Galetti [a], John Townend [b], Stephen Bannister [c]

[a] School of GeoSciences, University of Edinburgh, Edinburgh EH9 3JW, United Kingdom
[b] School of Geography, Environment and Earth Sciences, Victoria University of Wellington, Wellington 6012, New Zealand
[c] GNS Science, Lower Hutt 5040, New Zealand

ARTICLE INFO

Article history:
Received 30 October 2011
Received in revised form
3 June 2012
Accepted 5 June 2012
Editor: P. Shearer

Keywords:
interferometry
seismology
observational science
seismogram
phase velocity
causality

ABSTRACT

We show that interferometric theory allows recordings on a large variety of sensor types to be both spatially and temporally redatumed. Recordings of an energy source can thus be obtained at times before, during or after the period during which the sensor was physically installed. As a consequence, sensors in acoustic, elastic, electromagnetic, electrokinetic and a variety of other wavefield or diffusive environments may be deployed retrospectively, after an event of interest occurs and at locations chosen with the benefits of hind-sight: recordings of the event of interest can then be constructed post hoc. As an illustration, seismograms from two earthquakes are constructed on a seismometer deployed only after the earthquakes' seismic energy had completely dissipated. Bizarrely, a contributory component of such deterministic seismograms turns out to be ambient, random seismic noise. The seismograms obtained can be used to estimate seismic velocities in the vicinity of the seismometer, and provide independent information about the source phase (which is unavailable from the equivalent direct recordings). Thus, such retrospective observations provide novel information about both the earth and the energy source.

1. Introduction

Causality in observational science appears to require that any particular sensor be installed before a system is perturbed in order for it to measure the resulting energy fluctuations. This would imply, for example, that a seismometer must be installed and be active before an earthquake occurs if the resulting earthquake seismograms are to be recorded. In this article we show that this is untrue: as long as other sensors record the signals of interest directly, recordings of fluctuations from any energy source can be obtained on a newly installed sensor whether the source event occurred before, during, or after the period of that sensor's physical installation. Seismometers could therefore be deployed after an earthquake occurs, and still record that earthquake.

Although this result is counter-intuitive, we show that such measurements can be made in practice by using the theory of wavefield interferometry. With its foundations (for thermal fluctuations) already recognisable in the Fluctuation Dissipation Theorem (Greene and Callen, 1951; Callen and Welton, 1951), interferometric theory was developed almost independently in the fields of acoustics and ultrasonics (Cassereau and Fink, 1993; Weaver and Lobkis, 2001; Derode et al., 2003a, b), electromagnetics (Slob et al., 2007; Slob and Wapenaar, 2007), and seismology (Claerbout, 1968; Rickett and Claerbout, 2000; Campillo and Paul, 2003; Wapenaar, 2004; van Manen et al., 2005, 2006; Wapenaar and Fokkema, 2006). Subsequent generalised formulations span all of these regimes, as well as diffusive, dissipative and electrokinetic phenomena (Wapenaar et al., 2006; Snieder et al., 2007). Introductions to interferometric theory and reviews of much of the previous literature are given in Curtis et al. (2006), Wapenaar et al. (2010a, b), and Galetti and Curtis (2012).

Interferometry refers in a broad sense to methods of correlation, convolution or deconvolution of recordings that translate data into signals that would have been recorded at positions other than those at which sensors were deployed (Hong and Menke, 2006; Curtis et al., 2009), or into signals that would have been recorded if energy sources had existed at locations other than those of the sources (all other references cited above). We can therefore generally describe most interferometric methods derived to date as performing spatial redatuming. This has resulted in extraordinary advances in seismic imaging at global, regional or industrial scales (e.g., Shapiro et al., 2005; Sabra et al., 2005; Gerstoft et al., 2006; Moschetti et al., 2007; Lin et al., 2007;

* Corresponding author.
E-mail address: andrew.curtis@ed.ac.uk (A. Curtis).

0012-821X/$ - see front matter © 2012 Elsevier B.V. All rights reserved.
http://dx.doi.org/10.1016/j.epsl.2012.06.008

Yang et al., 2007; Halliday et al., 2008; Ruigrok et al., 2010; Nicolson et al., 2011; Behr et al., 2011), in acoustics (e.g., de Rosny and Fink, 2002; Derode et al., 2003a, b), in synthetic or computational modelling (van Manen et al., 2005, 2006, 2007), in the derivation of new optical theorems (Snieder et al., 2008; Halliday and Curtis, 2009; Douma et al., 2011) and new algorithms for imaging (Thorbecke and Wapenaar, 2007; Halliday and Curtis, 2010; Vasconcelos et al., 2010), velocity analysis (Mikesell et al., 2009; King et al., 2011; King and Curtis 2011, 2012) and noise removal (Curtis et al., 2006; Halliday et al., 2010, 2007; Sens-Schönfelder, 2008), in constructing measured seismograms in the Earth's deep subsurface where no sensors are located (Hong and Menke, 2006; Curtis et al., 2009), in monitoring tiny changes in the Earth's properties (Brenguier et al., 2008) and in a variety of other fields (Wapenaar et al., 2010a, b).

In this paper, we show that a recent advance in interferometric theory allows simultaneous spatial and temporal redatuming. In other words, recordings of energy fluctuations in a medium using sensors active during one interval of time can be used to derive recordings of equivalent data that would have been recorded at different spatial locations and at different times—before, during or after the period of physical installation of the sensor at the new location. Thus, if an event of interest occurs, a sensor can thereafter be deployed at a location where, in retrospect, one would have liked to have had recordings; the desired recordings can then be synthesised directly from physically recorded data using the methods described here, without recourse to synthetic or physical modelling of the medium.

As an example, we construct retrospective observations of seismograms from two earthquakes on a seismometer that was not deployed until after the earthquake-derived seismic wavefield fluctuations had subsided. These seismograms are used to estimate seismic velocities in the vicinity of the new seismometer, showing that novel information about the real Earth is obtained using this method. In another counter-intuitive result we show that the key to constructing recordings of such deterministic fluctuations from spatio-temporally impulsive earthquake sources is to make use of recordings of ambient field fluctuations from spatially- and temporally-distributed and incoherent sources (i.e., random 'noise').

In what follows we introduce the theory of retrospective observation, and the various approximations necessary to apply it in practical situations. The example introduced above is then presented in detail, demonstrating that in practice the approximations invoked do not require overly restrictive conditions, and that the method creates acceptably accurate and informative results. This is followed by a discussion of both alternative interpretations and various implications of the method including an illustration of how novel, independent information about the source may be obtained, before concluding by summarising the principal advances described herein.

2. Method

The key to this method is to propagate wavefields recorded at one set of receivers from an event of interest (e.g., an earthquake) onto a receiver at which the event was not recorded, using propagators determined from seismic interferometry. We show below that this can be achieved by using the new theory of *source–receiver interferometry*. However, since that theory is difficult to assimilate at a first reading, we begin with a simple analogy for how the method works from the field of geodetic surveying, then demonstrate intuitively how this is achieved in seismology for a particular simple synthetic scenario. This scenario pertains to one of three canonical geometries for source–receiver interferometry, and is the one that we use later in this paper to obtain retrospective earthquake seismograms.

Suppose one conducts a geodetic survey to measure the elevation of a mountain, a survey that includes point Q but which does not measure the elevation at a certain point P. If later we measure the elevation of P relative to the point Q (at which one has already measured the elevation), the absolute elevation at point P can be determined, even though it was not measured directly in the original survey. Importantly, the relative measurement of the elevation of P relative to point Q can be made at any point in time—before, during or after the original geodetic survey, provided the mountain's topographic profile did not change during the intervening period. The technique proposed in this paper uses the same principle, but it is applied in a more complicated way because it involves dynamic fields.

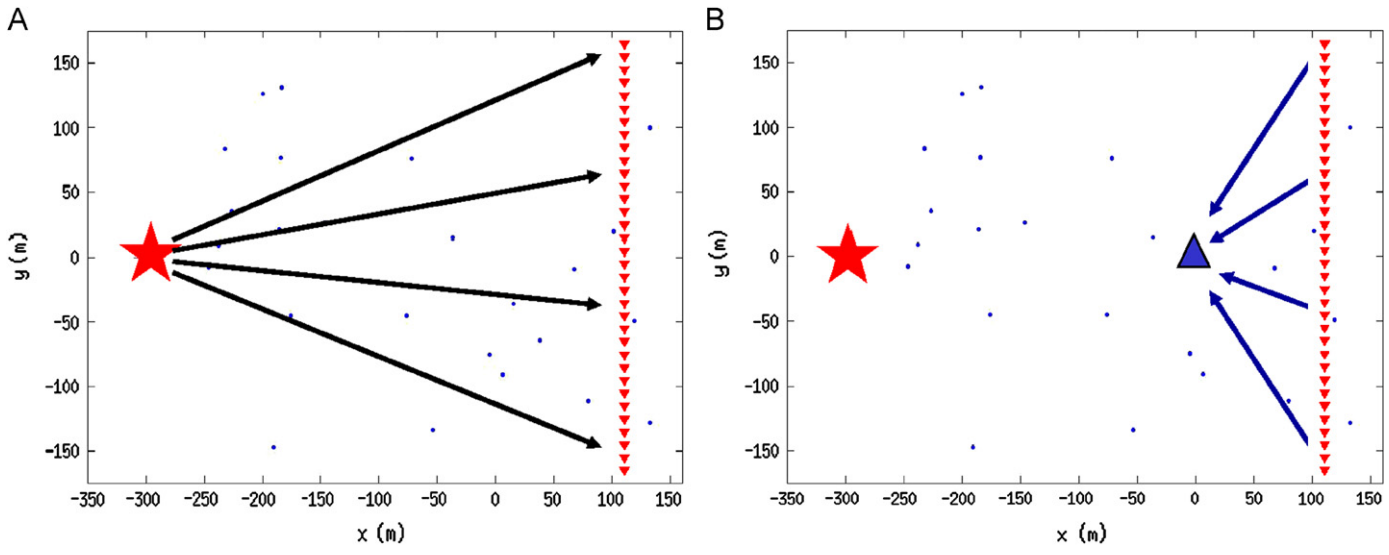

Fig. 1. Schematic overview of the first two steps involved in one form of the method. (A) Geometry of energy source (star), semi-permanent receivers (red triangles), and point scatterers (dots). The source is recorded on each of the receivers, as denoted by the black arrows. (B) At any time before, during or after the source event in A, a new sensor is installed (blue triangle). Green's functions are calculated between the location of each red sensor and the blue sensor (denoted by blue arrows). These Green's functions are used as projection operators, to project the data recorded in A to the new receiver location in B. (For interpretation of the references to colour in this figure legend, the reader is referred to the web version of this article.)

Fig. 1A shows a simple geometry of a source and an array of receivers. We use this example to illustrate the steps involved in applying the method to dynamic fields. These receivers (red) are regarded as semi-permanent—in seismology they would be regarded as part of the backbone array of seismometers used to monitor seismic activity over long time periods. When the source occurs, it is therefore recorded in real time by that array of receivers, and we refer to this as step 1 of the method which is equivalent to conducting the original geodetic survey in the analogy above. Synthetic seismograms for the particular geometry of scatterers shown in an otherwise homogeneous medium are illustrated in black in Fig. 2.

In step 2, which may take place at any time before, during or after step 1, a new (blue) receiver is located in a position where we would like to make recordings as shown in Fig. 1B. During its period of installation, the inter-receiver Green's functions between the location of each individual semi-permanent receiver and the new receiver are estimated. These are the recordings that would be observed at the blue location if an impulsive source was fired at any of the red locations, and may be estimated by an application of standard, ambient-noise seismic interferometry. Once this has been achieved, the new (blue) receiver may be removed.

Step 2 is equivalent to recording the relative heights of points P and Q in the analogy above. This relative measurement is like a transfer function that allows an absolute height measurement at Q to be 'projected' into an absolute height at P. Similarly in the seismological example, at any time after steps 1 and 2, in step 3 the inter-receiver Green's functions created above may be used as transfer functions, to project the recordings of the source made at the red receivers to construct the data that would have been recorded at the blue seismometer location if that sensor had been recording at the time of the event (the blue trace in Fig. 2). This compares well with the real seismogram that would have been recorded (and which here has been directly modelled) which is shown in red. Thus, the method yields new information that may be useful, for example, either to characterise the medium locally around the new receiver location or to characterise the source event.

The three steps described schematically above are embodied within the theory of source–receiver interferometry (Curtis and Halliday, 2010). This theory shows that a Green's function denoted $G(\mathbf{r},\mathbf{s})$ between a source at location $\mathbf{s}$ and a sensor at $\mathbf{r}$ can be synthesised, given recordings at distributed sensors on one closed

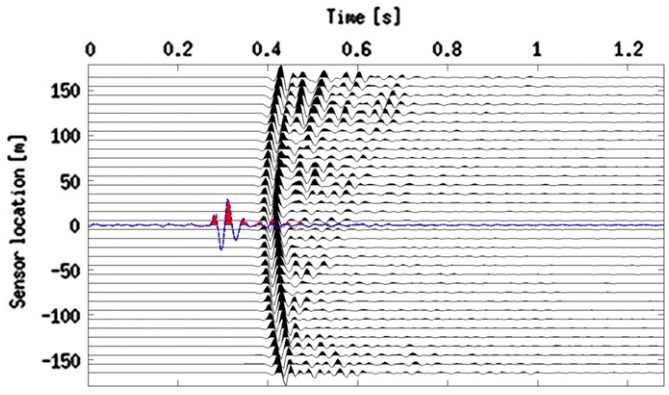

Fig. 2. Step 3 of the method—constructing the new recording: originally recorded wavefield responses at the line of red receivers in Fig. 1A (black waveforms), and the new seismogram at the blue receiver in Fig. 1B (blue waveform) overlain on the directly-modelled waveform at that receiver (black line with red fill). These latter two waveforms are amplified by a factor of 2 for ease of comparison. (For interpretation of the references to colour in this figure legend, the reader is referred to the web version of this article.)

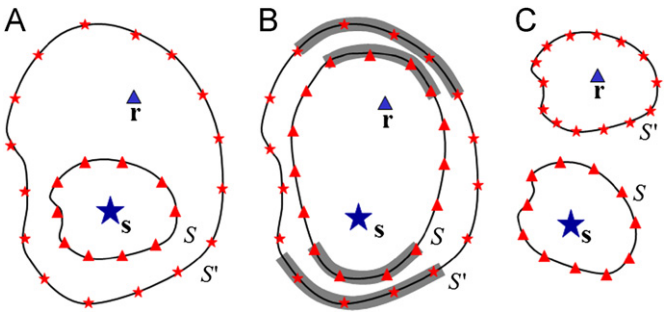

Fig. 3. Canonical geometries for which Curtis and Halliday (2010) provide acoustic and elastic interferometric formulae. Triangles represent receivers, stars represent sources. The blue star at **s** represents the main source location (the earthquake in the example), and the blue triangle **r** represents one of the blue receivers in Fig. 5 or Fig. 1. The thick grey lines in B show schematically those sections of the boundaries within which the integrands of Eqs. (1) and (2) become approximately stationary for waves that are not strongly scattered. (For interpretation of the references to colour in this figure legend, the reader is referred to the web version of this article.)

boundary, of sources distributed on a second closed boundary (Fig. 3; see also Curtis, 2009; Curtis and Halliday, 2010; Halliday and Curtis, 2010). We rewrite the interferometric equations from Curtis and Halliday (2010) in the following way:

$$G_H(\mathbf{r},\mathbf{s}) \cong \frac{2jk}{\omega\rho}\int_S G^*(\mathbf{s},\mathbf{x})G(\mathbf{r},\mathbf{x})d\mathbf{x} \tag{1}$$

where

$$G_H(\mathbf{r},\mathbf{x}) \cong \frac{2jk}{\omega\rho}\int_{S'} G^*(\mathbf{x},\mathbf{x}')G(\mathbf{r},\mathbf{x}')d\mathbf{x}' \tag{2}$$

All equations herein are expressed in the frequency domain, and the canonical geometry assumed in these equations is shown in Fig. 3B. Eqs. (1) and (2) represent propagation of waves of wavenumber k and angular frequency ω in an acoustic medium of density ρ which, in these equations, is assumed to be approximately constant at the boundaries S and S'. Here $j=\sqrt{-1}$ and * denotes complex conjugation, so G^*G is the frequency-domain representation of cross-correlation.

For any Green's function G, the so-called homogeneous Green's function on the left hand side of Eqs. (1) and (2) is defined to be $G_H=G+G^*$. Since complex conjugation in the frequency domain corresponds to time-reversal in the time domain, G can be obtained from G_H by taking positive times only, provided no energy arrives instantaneously (at zero time) in G. Variables $\mathbf{x}$ and $\mathbf{x}'$ represent locations on sensor boundary S and source boundary S', respectively.

More generally, Eqs. (1) and (2) together describe one form of the method of source–receiver interferometry, so-named because, unlike other forms of interferometry, it can be used to construct a Green's function between a source and a receiver rather than between a pair of sources or a pair of receivers. Other canonical geometries for which equivalent source–receiver interferometric theories exist are illustrated in Fig. 3A and C: formulae corresponding to Eqs. (1) and (2) for each of these cases may be derived from those given in Curtis and Halliday (2010); corresponding expressions for purely scattered waves may be obtained from those given in Halliday and Curtis (2010).

Using Eqs. (1) and (2) together to calculate the new, desired seismogram corresponds to step 3 of the method as described above. Individually however, Eqs. (1) and (2) each describe standard forms of interferometry used for spatial redatuming in most previous studies, including those cited above. The Green's functions on the right side of each equation have source locations distributed over an arbitrary surrounding surface, and these are

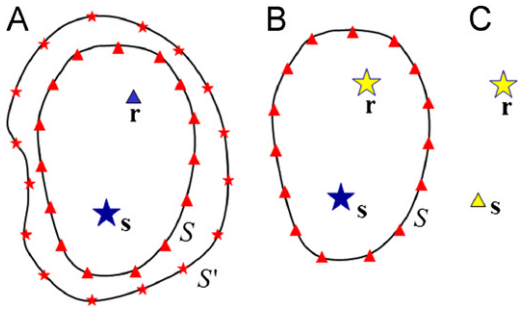

Fig. 4. Steps involved in source–receiver interferometry. (A) As in Fig. 3B, a source and a receiver are surrounded by two surfaces, one of receivers and one of sources. (B) Using Eq. (2), the outer surface of sources is used to calculate the Green's functions between the receiver at position **r**, and all other receivers on surface *S*. This in effect turns the receiver at **r** into a virtual source, the signal from which is recorded on *S*. (C) The geometry in B is exactly the geometry used for inter-source interferometry (Curtis et al., 2009), whereby the Green's function between **r** and **s** is calculated using Eq. (1), effectively turning the source at **s** into a virtual receiver. Key as in Fig. 3; yellow symbols represent virtual sources and receivers.

redatumed to a Green's function from a single, spatially-localised source location given on the left.

The steps taken in source–receiver interferometry (approximated in Eqs. (1) and (2)) are illustrated in Fig. 4. Mathematically, Eq. (2) would be employed first: this uses the outer boundary of sources in Fig. 4A and the standard form of inter-receiver interferometry to calculate the Green's functions between the receiver at **r** and all other receivers on boundary *S* (this corresponds to calculating the Green's functions denoted by blue arrows in Fig. 1B, hence step 2 of the method as described above). In effect, this converts the receiver at **r** into a so-called virtual source (Fig. 4B) which is recorded at all other receivers. Thereafter, the geometry in Fig. 4B is one of the canonical geometries for inter-source interferometry (Curtis et al., 2009), and can be used with Eq. (1) to calculate the Green's function between **r** and **s**, thus converting the source at **s** into a virtual receiver (Fig. 4C). In the description of the method above, this latter application of interferometry assumes that step 1 in Fig. 1A (recording the waveforms shown in black in Fig. 2 and denoted (in reciprocal form) by $G(\mathbf{s},\mathbf{x})$ in Eq. (1)) has been completed at any previous time. Calculating the right side of Eq. (1) then completes step 3 of back-projecting this waveform data to the new, blue receiver location shown in Fig. 1B, to provide the waveform $G(\mathbf{r},\mathbf{s})$ shown in blue in Fig. 2.

While Eqs. (1) and (2) are individually nothing more than representations of spatial redatuming, it is the coupling of Eqs. (1) and (2) in source–receiver interferometry that allows a form of temporal redatuming. Crucially, notice that recordings of the source at **s** appear in Eq. (1) only, and direct recordings at the sensor **r** appear in Eq. (2) only. The source at location **s** needs never to be recorded directly by the sensor at arbitrary location **r**, yet $G(\mathbf{r},\mathbf{s})$ can still be recovered from Eq. (1). This is true even if the source occurred outside the time-interval of operation of the sensor at **r**, and hence calculating $G(\mathbf{r},\mathbf{s})$ corresponds to apparent spatio-temporal redatuming. The underlying requirements are that other distributed sources (on boundary *S'* in Figs. 3 and 4) are recorded at **r**, and that other sensors (on boundary *S*) recorded both the distributed and the localised sources. It is also assumed that the Green's functions between the receiver location **r** and the other receivers (calculated using Eq. (2)) do not change between the time period of the data used for their calculation, and the time at which the source at **s** was recorded on the boundary of receivers.

Eqs. (1) and (2) are each approximations of cross-correlational interferometry derived for the case of acoustic wave propagation at high frequencies by assuming that the medium outside each surface is approximately homogeneous and isotropic, and that the surface *S'* is large and spherical (Wapenaar and Fokkema, 2006). Appendix A provides corresponding exact acoustic expressions for arbitrary boundary surfaces and the exact forms for elastic regimes are given in Curtis and Halliday (2010) for correlational and convolutional/deconvolutional interferometry. Similar results can be derived for electromagnetic, electrokinetic, diffusive, and other regimes using the results in the references cited for each of these regimes in Section 1. This temporal redatuming technique is therefore applicable in many domains of observational science.

When synthetic data are available, the method of source–receiver interferometry has been shown to work exactly if the exact equations in Appendix A are used (Curtis and Halliday, 2010; Halliday and Curtis, 2010). However, in many practical situations assumptions of both the completeness and closure of source or receiver boundaries, and of the uniformity of media surrounding each boundary, are violated. It has nevertheless been shown in numerous synthetic, laboratory and field studies that useful results may still be obtained from approximations 1 or 2 (de Rosny and Fink, 2002; Shapiro et al., 2005; van Manen et al., 2005, 2006; Wapenaar, 2006). In particular, provided that the amplitudes of wavefields around the boundaries do not vary abruptly in space, the integrals in either equation can be simplified using the stationary phase approximation (Snieder, 2004). This states that the dominant contribution to either integral is from regions of *S* or *S'*, within which the phase of the corresponding integrand is approximately stationary with respect to position on the boundary. If the medium is not too strongly scattering, stationary regions for the homogeneous Green's function $G_H = G + G^*$ occur for sources or receivers within the areas outlined schematically in grey in Fig. 3B. To span stationary regions for Green's functions G or G^* individually requires only sources and receivers on the top two surfaces, or on the bottom two surfaces in that diagram, respectively (Snieder, 2004). We make use of this in the seismological example below.

In practice, it may be the case that the required Green's functions $G(\mathbf{x},\mathbf{x}')$ between sources and receivers on the two boundaries were not recorded directly. Nevertheless, field fluctuations from ambient sources at distributed locations $\mathbf{x}'$ on an arbitrary surface *S'* may still be recorded by sensors at locations **x** on boundary *S*, and at **r**. Such field fluctuations from different sources overlap temporally and hence do not yield direct recordings of the Green's functions $G(\mathbf{x},\mathbf{x}')$ and $G(\mathbf{r},\mathbf{x}')$ required in Eq. (2). However, Wapenaar and Fokkema (2006) showed that if ambient sources are assumed to be mutually uncorrelated in time then the right side of Eq. (2) is given approximately by cross-correlation of ambient fluctuations v recorded at locations **x** and **r**:

$$G_H(\mathbf{r},\mathbf{x}) \cong C v(\mathbf{x}) v^*(\mathbf{r}) \tag{3}$$

for some constant *C*. Thus, spatio-temporal redatuming can also be achieved using ambient noise fields. Since Eq. (3) makes no reference to the time of occurrence of the event of interest, the noise field can be recorded before, during or after that event.

Given the successive approximations involved in arriving at Eqs. (1) and (2) and particularly (3) from the exact expressions in Appendix A, it might appear that the compounding of errors would overwhelm any useful signal in Green's functions estimates in practice. To allay this suspicion, we now employ all of the above approximations in a practical geophysical example and obtain robust estimates of useful wavefield and medium properties that are not available from direct recordings of the source alone. This example also illustrates how band-limited data recordings observed in nature from real sources with arbitrary, extended time functions (rather than the impulsive sources assumed in the Green's function representations above) can be estimated.

3. Example: retrospective earthquake seismograms

We demonstrate the method of retrospective observation using real data by synthesising seismograms from two earthquakes that occurred in New Zealand, on a seismometer that was not operational at the time of either earthquake. In order to assess the accuracy of the method, we also construct seismograms on a set of other seismometers that were operational at the time of the two earthquakes, and on which the seismic wavefield from each earthquake was recorded directly. This allows a direct comparison of measured and reconstructed seismograms

In this case, no boundary S' of active impulsive sources is available, so we apply the ambient fluctuation approximation in Eq. (3). A variety of ambient sources exist in this case (oceanic waves, wind, anthropogenic activity) at distributed and unknown locations $\mathbf{x}'$. Oceanic wave sources are expected to occur around the coast (Fig. 5), whereas wind-derived sources may be more spatially distributed occurring on-shore as well as off-shore (Brooks et al., 2009). The form of surface S' therefore remains unknown, but can reasonably be assumed to be extremely irregular; such irregularity has been shown to improve the accuracy of approximations made in moving from Eq. (2) to Eq. (3) (Wapenaar, 2006).

Resulting fluctuations in the seismic wavefield were recorded by backbone seismometers at locations $\mathbf{x}$ in the section of boundary S assumed to include the positions of stationary-phase of the integrand in Eq. (2) (Fig. 3). In order to obtain a good approximation from Eq. (3), we use six months of ambient noise recordings at stations in the Central North Island Passive Seismic Experiment (CNIPSE; Reyners et al., 2006), a period typically used in seismological ambient interferometric studies (e.g. Lin et al., 2007). Since in practice we do not know the value of the constant C, the amplitudes of signals resulting from the method remain unknown and are henceforth ignored.

For each earthquake, an approximation to $G(\mathbf{x},\mathbf{s})$ needs only be recorded on the permanent (red) receivers at locations $\mathbf{x}$. In practice these recordings are always band-limited due to the attenuation of high frequencies, as are the recorded ambient-source field fluctuations $v(\mathbf{x})$ used in Eq. (3). The desired earthquake seismograms that would be recorded by the temporary (blue) receiver array may be synthesised only within the frequency band spanned by both the recorded data and the ambient source field fluctuations—between 10 s and 20 s period in this example.

Additionally, as is the case for many real world sources, energy released from earthquakes may have a non-instantaneous time dependence—here represented in the frequency domain by $T(\omega)$. In such cases, instead of $G(\mathbf{x},\mathbf{s})$ (used in Eq. (1) in reciprocal form), the boundary sensors record $T\,G(\mathbf{x},\mathbf{s})$. Pre-multiplying Eq. (1) by T^* and applying source–receiver reciprocity gives

$$T^*G_H(\mathbf{r},\mathbf{s}) \cong \frac{2ik}{\omega\rho}\int_S [TG(\mathbf{x},\mathbf{s})]^*G(\mathbf{r},\mathbf{x})d\mathbf{x} \tag{4}$$

Thus we see that if real recordings $TG(\mathbf{x},\mathbf{s})$ are used in place of $G(\mathbf{s},\mathbf{x})$ in Eq. (1), the result is $T^*G_H(\mathbf{r},\mathbf{s}) = T^*G(\mathbf{r},\mathbf{s}) + T^*G^*(\mathbf{r},\mathbf{s})$. In the time domain the result therefore has T^*G at positive times and

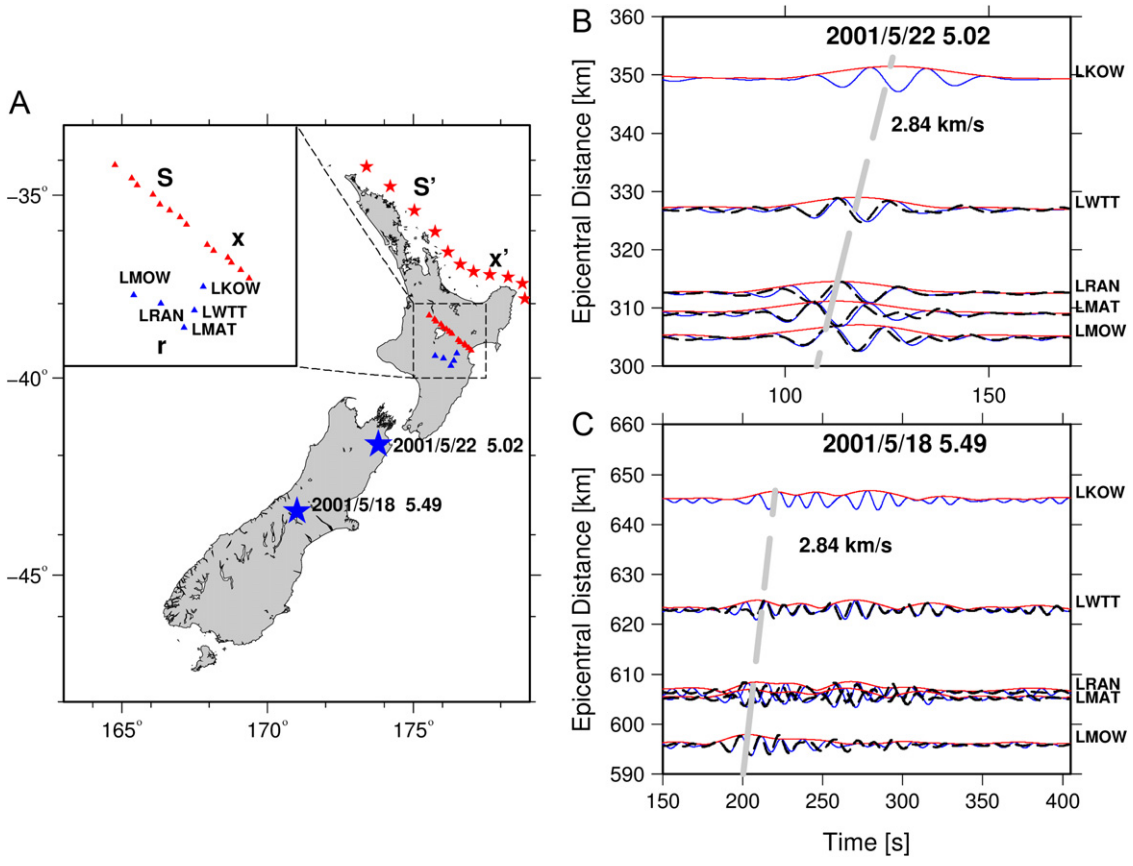

Fig. 5. (A) Two New Zealand earthquakes at locations $\mathbf{s}$ (blue stars), with magnitudes 5.0 and 5.5. These were recorded by distributed sensors at locations $\mathbf{x}$ (red triangles) on surface S (see inset). Ambient noise sources (some represented by red stars) occur at locations $\mathbf{x}'$ on surface S' which remains unknown throughout this example. (B) and (C) Seismograms (blue) synthesised using Eqs. (1) and (3) at the five sensor locations $\mathbf{r}$ and their envelopes (red) for each earthquake, band-limited to 10–20 s period. Actual recordings are also shown (dashed). Dashed linear gradients indicate seismic wave propagation velocities of 2.84 km/s. (For interpretation of the references to colour in this figure legend, the reader is referred to the web version of this article.)

T^*G^* at negative times. However, $T^*G(\mathbf{r},\mathbf{s})$ is not the desired recording at location $\mathbf{r}$ as the source–time dependence T is reversed in time. In real applications, only the negative-time part of the result, T^*G^*, should therefore be used as, after time-reversal (complex conjugation), it gives TG which represents the source–time dependence correctly.

In Fig. 5, seismograms are synthesised at blue seismometers, and real recordings at the same seismometers are shown within the same period band for comparison. For both earthquakes, the main arrival is constructed well, and synthesised seismograms from the larger earthquake match direct measurements far into the coda. The most northerly blue seismometer, LKOW, was not operational until days after the seismic waves from both earthquakes had dissipated. Hence, the illustrated seismograms at LKOW are truly constructed at a seismometer location selected retrospectively—after the event. In other words, we have shown that robust estimates of unrecorded and spatio-temporally redatumed seismograms may be made in practice despite the various theoretical approximations employed.

4. Discussion

While the method is not restricted to surface waves in principal (all equations above and in the appendix are also valid for body waves), the fact that the backbone array of receivers is restricted to the surface of the Earth, and that the dominant sources of ambient noise occur relatively close to the Earth's surface, results in the dominance of surface wave energy in the seismograms constructed in the above examples (e.g., see Forghani and Snieder, 2010). The linear move-out of the first-arriving envelope peak (Fig. 5) therefore provides a measure of the speed of surface wave propagation across the blue seismometer array. Using only seismograms reconstructed from the above equations, both earthquakes yield consistent best-fit velocities of 2.8 km/s to two significant figures, which also matches the estimate from the available direct recordings (Lin et al., 2007; Behr et al., 2011). This demonstrates that even if all of the blue seismometers had been installed long after both earthquakes had occurred, or if they had been switched off at the time of both earthquakes, the energy from either earthquake could be used to find medium properties localised around the blue seismometer array. This would not be possible using only recordings on the red seismometer array without relying on extensive synthetic modelling and necessarily making assumptions about the medium properties between the red and blue seismometers. In other words, the method of retrospective observation provides new information about the medium compared to that contained in the original recordings on the backbone array.

Intriguingly, further new information is offered by Eq. (4). When the source event has a non-impulsive source time signature T, the causal part of the reconstructed seismograms consists of T^*G, whereas the acausal part gives T^*G^*. Here, G is the true (band-limited) event-to-receiver Green's function, and for notational convenience we have dropped the positional arguments $\mathbf{r}$ and $\mathbf{s}$ on the left hand side of Eq. (4). Let us define $C=T^*G$ to be the signal on the causal side, $A=T^*G^*$ to be the signal on the acausal side, where both are defined in the frequency domain and are in general complex. Additionally, let $T=|T|e^{it}$ and $G=|G|e^{ig}$ where t is the phase of T and g is the phase of G. We then find the relation $C/A=e^{i2g}$. That is, by calculating C/A we estimate a quantity of unit amplitude and (twice) the phase g of the true Green's function G between the real source and the new receiver, without contamination from the phase of the source time function T. If we insert this estimate of g back into our measurements of either A or C, we can re-arrange to obtain, for example, $e^{ig}C^*/|C|=e^{it}$. This provides an independent estimate of the phase of the source time function t.

Fig. 6 shows the various estimates of t for each of the earthquakes used in this study (note the standard 2π phase-wrap in this figure). Since we obtain one such estimate from each new seismometer location, the variations in phase between different seismometers also provides an estimate of the uncertainty in the source phase. Thus, for example, we see that other than station LMOW the source phase of the second earthquake (lower plot in Fig. 6) is consistently estimated across a large portion of the frequency range considered.

Measuring the Green's function phase g is desirable in order to obtain surface wave phase velocity estimates along event-to-station paths. Such measurements are commonly used to perform surface wave tomography. However, phase velocity data are usually contaminated with inaccuracies in estimates of the source time function phase t, since standard seismometers record only the combination TG. Neither T nor G are known independently from one another, and independent estimates of t and g must be made using inverse theory. The ability to estimate t independently from g without using inverse theory shows that our

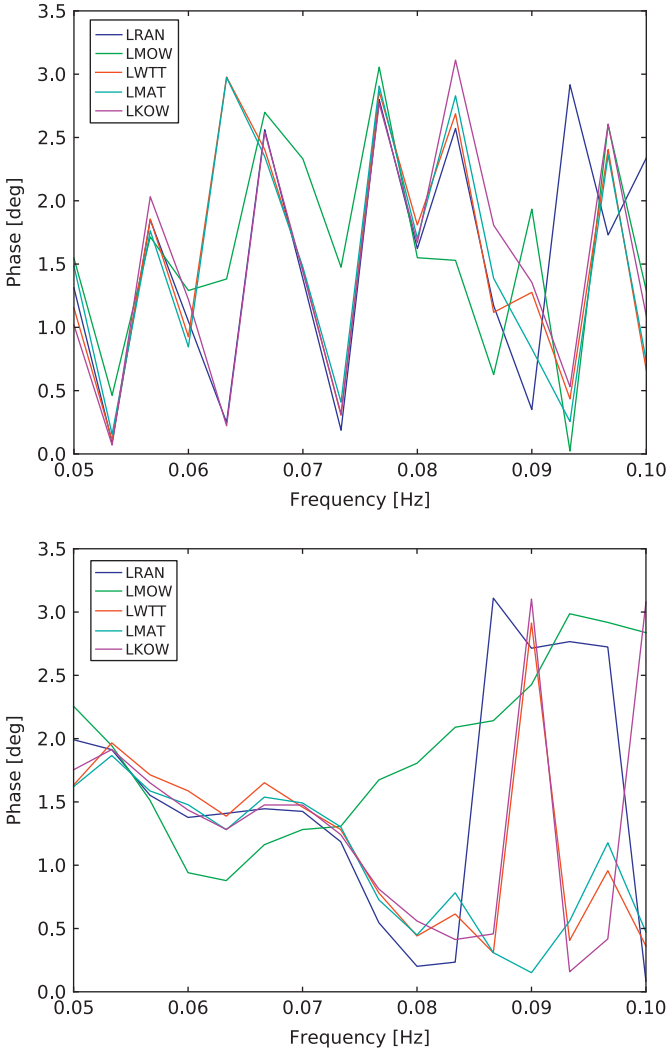

Fig. 6. Estimates of source phase as a function of frequency for the 2001/05/18 earthquake (top) and 2001/05/22 earthquake (bottom). Each curve is derived from the two terms on the left hand side of Eq. (4) using the method outlined in the Discussion for a different temporary seismometer. The variation in estimates between different seismometers provides a measure of uncertainty in the phase estimates.

method provides new information that is not directly available from conventional seismometer recordings.

One can think of Eqs. (1) and (2) as approximations to a particular case of Green's theorem in mathematics (Morse and Feshback, 1953). For example, in the context of interferometry, Ramirez and Weglein (2009) show that if a continuous field and its normal derivative are known on a closed boundary S then, under certain circumstances, Green's theorem can be used to project or interpolate the wavefield to any point in the medium enclosed by the boundary. What is novel in the current application is the demonstration that this is possible even if the projection operators, namely the Green's functions $G(\mathbf{r},\mathbf{x})$ in Eq. (1), are obtained only after the boundary recordings on S have been made (using Eq. (2)). Under this interpretation, these projection operators are derived from an application of standard interferometry (Eq. (2)) using a boundary of sources S'. Crucially the latter sources can be active at different times from the occurrence of the original continuous field, provided that the medium did not change in the intervening period. Of course, if estimates of the projection operators (in our case derived from ambient noise) are inaccurate then the projection will be inaccurate also. However, the above real-data examples show that the various approximations and estimates employed still result in robust estimates of the (measured) source-to-receiver seismograms.

The equations herein are all derived for acoustic media with no attenuation of wave energy. While alternative derivations have been proposed for attenuating media, they are not easy to apply in practice as they require the injection of source energy throughout the volume of the medium to compensate for wave energy lost during propagation (Snieder, 2007). However, the examples herein show that the method appears to be robust to this assumption: the backbone array in Fig. 5 traverses directly across the Taupo Volcanic Zone, the region of highest known seismic attenuation in New Zealand (e.g., Brooks et al., 2009; Behr et al., 2011). Nevertheless, the seismograms constructed interferometrically show an excellent match to real seismograms where the latter were recorded. Of course, the absolute amplitudes of recorded seismograms are not recovered using this method, but since the envelopes of the constructed and recorded signals match well, the relative amplitude of different phases appears to be estimated robustly within the frequency band considered. A similar quality of match of constructed and measured seismic envelopes was also observed across the Western United States by Curtis et al. (2009) for the case of inter-source interferometry, where again semi-impulsive earthquake sources were used and their seismograms reconstructed at new measurement (virtual sensor) locations. Hence, it appears that at least in these various cases studied, even strong attenuation does not seem to affect the results as severely as might be expected.

Other work that is most closely related to ours includes Stehly et al. (2008) who convert a backbone array of distributed stations into a set of virtual sources which in turn are used to replace missing ambient noise sources when estimating inter-receiver Green's functions. Using a method closely related to that of Stehly et al. (2008), Ma and Beroza (2012) showed that conventional inter-receiver ambient noise interferometry can be performed even if each pair of receivers were not contemporaneously active; they show that a link between the asynchronous recordings at the two stations can be made by converting a backbone array of other receivers into virtual sources.

The important implications of our work for seismology over previous studies are that seismometers may be installed in locations for which we would ideally have liked to have had sensors that record either natural or induced source events that occurred in the past, or where we might like to have those measurements at future times. A useful instance of this would be to place seismometers closer to earthquake hypocentres than those that were recording at the time of the event (indeed, the example above is an instance of this). Such sensors can be placed at locations chosen retrospectively using the benefits of hindsight about where the event of interest occurred. Similar applications might occur in laboratory experiments, for example, in which local measurements of material failures are desired, but where the location of the failure is not known *a priori*. Alternatively, we might 'prepare' a measurement location for some possible future event by placing a sensor at the location, estimating the required Green's functions from the backbone array to that location, and then remove the sensor. Thereafter, measurements could still be made at that location provided the Green's functions to the backbone array did not change.

In seismology it may in fact be possible to obtain many new seismograms from old earthquakes simply by using new sensors that have been installed subsequent to the events' occurrence. Seismometer arrays around the world have been updated, expanded and densified as time progresses: it is likely that many modern seismometers have been sited in places at which we would like to have had recordings of earlier earthquakes. Depending on the geometric arrangement of the (backbone array) seismometers that were active at the time of the event, the method presented herein may in principle be used to reconstruct corresponding recordings at the new seismometer locations.

The ability to maintain active measurement capability at previously-occupied sites may have implications for survey or experimental design. In some monitoring situations it may be expedient to establish a permanent backbone of sensors in a geometry that best facilitates spatio-temporal redatuming. An example might be to install permanent sensors in either a linear

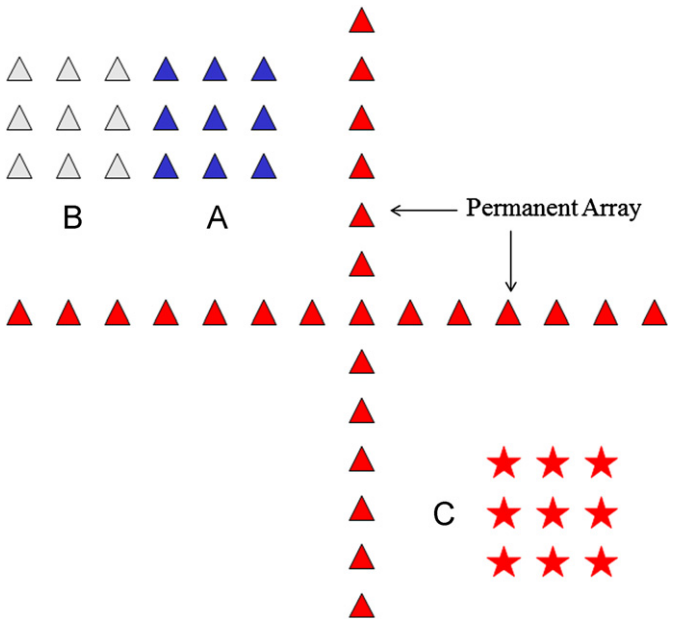

Fig. 7. Schematic diagram of how experiments might be designed in order to make use of the theory herein. A red permanent backbone array stays fixed, while the blue temporary array (A) is installed and activated for a sufficient length of time to estimate Green's functions between the temporary and permanent receiver locations by using ambient noise interferometry. The temporary array may then be moved to a new set of locations. (B) Previous locations of the temporary array (grey) remain points at which recordings can be constructed even after the array has been removed, by using the theory herein. (C) An alternative is to use a temporary source array in place of the temporary receiver array. Sources are fired sequentially and recorded by the permanent array; thus an approximation to the above Green's functions can be measured directly. (For interpretation of the references to colour in this figure legend, the reader is referred to the web version of this article.)

array as in the New Zealand example above, or (to ensure a better azimuthal performance) a cross-shaped array spanning the length and width of the area to be monitored (Fig. 7). A roving temporary array could then be installed successively at a set of other spatially-distributed locations at which we wish to establish a measurement capability (Fig. 7A). The temporary array needs only to occupy any set of positions long enough that the Green's functions between the temporary and permanent locations can be estimated. Thereafter the temporary array may be moved to the next set of desired locations; measuring capability will be maintained at the previous locations thereafter (Fig. 7B).

While the necessary period of installation of the temporary array may span some months in the case of regional seismology if ambient noise interferometry is used to estimate the temporary-to permanent-location Green's functions as above, when these Green's functions estimates can be obtained directly by firing sources (e.g., in exploration seismology) another option is available. Instead of installing a receiver at each temporary location, an impulsive source may be fired at that location (Fig. 7C); the recordings of each source on the permanent array provide direct estimates of all of the temporary- to permanent-location Green's functions that are required to project future or past recordings on the permanent array to each of the temporary source locations. Each source is thus converted to a virtual receiver that is available for future use.

Related methods can be constructed for electromagnetic, electrokinetic, diffusive and a variety of other regimes. It is therefore likely that retrospective observations will find applications in a wide variety of disciplines.

5. Conclusions

Recordings of energy sources may be converted (projected) into recordings at locations at which they were not originally recorded, and at times before, during or after the time of a sensor's physical installation. Such redatumed recordings yield useful properties of either the wavefield, the medium through which it propagated, or both. Seismograms are thus shown to be obtainable from seismometers installed long after an earthquake occurred, using retrospective knowledge of the earthquake's location. The particular two-sided nature of these so-constructed seismograms also allows the phase of the source, and that of the source-to-receiver Green's function to be estimated independently. Generalisations of this theory to many other regimes of energy propagation (electromagnetic, diffusive, dissipative, electrokinetic, etc.) imply that such retrospective observations are possible in many fields of science.

Appendix A

The response between a source and a receiver can be derived using pair-wise combinations of correlation- and convolution-type representation theorems. Exact formulae corresponding to Eq. (1) and (2) in the main article for wave propagation in an acoustic medium are (Curtis and Halliday, 2010)

$$G(\mathbf{r},\mathbf{s})+G^*(\mathbf{r},\mathbf{s})=\frac{-1}{j\omega\rho}\int_S \Phi(\mathbf{r},\mathbf{x})n_i\partial_i G(\mathbf{s},\mathbf{x})-n_i\partial_i\Phi(\mathbf{r},\mathbf{x})G(\mathbf{s},\mathbf{x})dS \qquad (5)$$

where

$$\Phi(\mathbf{r},\mathbf{x})=\frac{-1}{j\omega\rho}\int_{S'}\{G^*(\mathbf{r},\mathbf{x}')n_{i'}\partial_{i'}G(\mathbf{x},\mathbf{x}')-n_{i'}\partial_{i'}G^*(\mathbf{r},\mathbf{x}')G(\mathbf{x},\mathbf{x}')\}dS'. \qquad (6)$$

Here, $G(\mathbf{r},\mathbf{s})$ is the Green's function in the frequency domain representing the pressure at $\mathbf{r}$ due to a volume injection-rate density source at $\boldsymbol{s}$, n_j is the jth component of the normal vector on the boundary S, ∂_k denotes a spatial derivative in the k-direction, and ρ is the medium's density. Primed and unprimed quantities relate to the primed and unprimed boundaries respectively, and Einstein's summation principle for repeated indices applies throughout. As in the main article, recordings of the source at $\mathbf{s}$ and recordings by the sensors at $\mathbf{r}$ are decoupled by Eq. (5) and (6), allowing temporal change with respect to timing of the source and the receiver installation. This requires recordings of other sources at locations $\mathbf{x}'$ on boundary S', and a boundary S of receivers at locations $\mathbf{x}$.

Eq. (1) and (2) in the main article are obtained from Eqs. (5) and (6) by assuming high-frequency propagation, locally planar wave fronts, and Sommerfield radiation conditions at the boundary surfaces (Wapenaar and Fokkema, 2006): $\mp jkG=n_i\partial_i G$. Here "$-$" pertains to outgoing waves and "$+$" to incoming waves across the boundary. These conditions hold exactly if waves travel perpendicularly to the boundaries.

References

Behr, Y., Townend, J., Bannister, S., Savage, M.K., 2011. Crustal shear wave tomography of the Taupo Volcanic Zone, New Zealand, via ambient noise correlation between multiple three-component networks. Geochem. Geophys. Geosyst. 12 (3), Q03015, http://dx.doi.org/10.1029/2010GC003385.

Brenguier, F., Campillo, M., Hadziioannou, C., Shapiro, N.M., Nadeau, R.M., Larose, E., 2008. Postseismic relaxation along the San Andreas Fault at Parkfield from continuous seismological observations. Science 321 (5895), 1478–1481.

Brooks, L.A., Townend, J., Gerstoft, P., Bannister, S., Carter, L., 2009. Fundamental and higher-mode Rayleigh wave characteristics of ambient seismic noise in New Zealand. Geophys. Res. Lett. 36 (23)http://dx.doi.org/10.1029/2009GL040434.

Callen, H.B., Welton, T.A., 1951. Irreversibility and generalised noise. Phys. Rev. 83, 34–40.

Campillo, M., Paul, A., 2003. Long-range correlations in the diffuse seismic coda. Science 299, 547–549.

Cassereau, D., Fink, M., 1993. Focusing with plane time-reversal mirrors: an efficient alternative to closed cavities. J. Acoust. Soc. Am. 94, 2373–2386.

Claerbout, J.F., 1968. Synthesis of a layered medium from its acoustic transmission response. Geophysics 33, 264–269.

Curtis, A., Gerstoft, P., Sato, H., Snieder, R., Wapenaar, K., 2006. Seismic interferometry—turning noise into signal. Leading Edge 25 (9), 1082–1092.

Curtis, A., 2009. Source–Receiver Seismic Interferometry. Annual Meeting. Society of Exploration Geophysics, pp. 3655–3658.

Curtis, A., Halliday, D., 2010. Source–receiver wave field interferometry. Phys. Rev. E 81 (4), 046601.

Curtis, A., Nicolson, H., Halliday, D., Trampert, J., Baptie, B., 2009. Virtual seismometers in the subsurface of the Earth from seismic interferometry. Nat. Geosci. 2, 700–704, http://dx.doi.org/10.1038/NGEO615.

Derode, A., Larose, E., Campillo, M., Fink, M., 2003a. How to estimate the Green's function of a heterogeneous medium between two passive sensors? Application to acoustic waves. Appl. Phys. Lett. 83, 3054–3056.

Derode, A., Larose, E., Tanter, M., de Rosny, J., Tourin, A., Campillo, M., Fink, M., 2003b. Recovering the Green's function from field–field correlations in an open scattering medium. J. Acoust. Soc. Am. 113, 2973–2976.

de Rosny, J., Fink, M., 2002. Overcoming the diffraction limit in wave physics using a time-reversal mirror and a novel acoustic sink. Phys. Rev. Lett. 89, 124301.

Douma, H., Vasconcelos, I., Snieder, R., 2011. The reciprocity theorem for the scattered field is the progenitor of the generalised optical theorem. J. Acoust. Soc. Am. 129, 2765–2771.

Forghani, F., Snieder, R., 2010. Underestimation of body waves and feasibility of surface-wave reconstruction by seismic interferometry. Leading Edge 29, 790–794.

Galetti, E., Curtis, A., 2012. Generalised receiver functions and seismic interferometry. Tectonophysics 532-535, 1–26, http://dx.doi.org/10.1016/j.tecto.2011.12.004.

Gerstoft, P., Sabra, K.G., Roux, P., Kuperman, W.A., Fehler, M.C., 2006. Green's functions extraction and surface-wave tomography from microseisms in southern California. Geophysics 71 (4), SI23–SI31.

Greene, R.F., Callen, H.B., 1951. On the formulation of thermodynamic fluctuation theory. Phys. Rev. 83, 1231–1235.

Halliday, D., Curtis, A., van Manen, Dirk-Jan., Robertsson, J., 2007. Interferometric surface wave isolation and removal. Geophysics 72 (5), A69–A73.

Halliday, D., Curtis, A., 2009. Generalised optical theorem for surface waves and layered media. Phys. Rev. E 79, 056603.

Halliday, D., Curtis, A., 2010. An interferometric theory of source–receiver scattering and imaging. Geophysics 75 (6), SA95–SA103.

Halliday, D., Curtis, A., Kragh, E., 2008. Seismic surface waves in a suburban environment—active and passive interferometric methods. Leading Edge 27 (2), 210–218, http://dx.doi.org/10.1190/1.2840369.

Halliday, D., Curtis, A., Vermeer, P., Strobbia, C., Glushchenko, A., van Manen, D-J., Robertsson, J.O.A., 2010. Interferometric ground-roll removal: attenuation of direct and scattered surface waves in single-sensor data. Geophysics 75 (2), SA15–SA25, http://dx.doi.org/10.1190/1.3360948.

Hong, T.-K., Menke, W., 2006. Tomographic investigation of the wear along the San Jacinto fault, southern California. Phys. Earth Planet. Inter. 155, 236–248.

King, S., Curtis, A., 2012. Suppressing nonphysical reflections in Green's function estimates using source-receiver interferometry. Geophysics 77 (1), Q15–Q25. http://dx.doi.org/10.1190/GEO2011-0300.1.

King, S., Curtis, A., 2011. Velocity analysis using both reflections and refractions in seismic interferometry. Geophysics 76 (5), SA83–SA96. http://dx.doi.org/10.1190/GEO2011-0008.1.

King, S., Curtis, A., Poole, T., 2011. Interferometric velocity analysis using physical and nonphysical energy. Geophysics 76 (1), SA35–SA49. http://dx.doi.org/10.1190/1.3521291.

Lin, F.C., Ritzwoller, M.H., Townend, J., Bannister, S., Savage, M.K., 2007. Ambient noise Rayleigh wave tomography of New Zealand. Geophys. J. Int. 170 (2), 649–666, http://dx.doi.org/10.1111/j.1365-246X.2007.03414.x.

Ma, S., Beroza, G.C., 2012. Ambient-field Green's functions from asynchronous seismic observations. Geophys. Res. Lett. 39, L06301, http://dx.doi.org/10.1029/2011GL050755.

Mikesell, D., van Wijk, K., Calvert, A., Haney, M., 2009. The virtual refraction: useful spurious energy in seismic interferometry. Geophysics 74 (3), A13–A17, http://dx.doi.org/10.1190/1.3095659.

Morse, P.M., Feshback, H., 1953. Methods of Theoretical Physics. McGraw-Hill, New York, ISBN: 978-0070433168.

Moschetti, M.P., Ritzwoller, M.H., Shapiro, N.M., 2007. Surface wave tomography of the western United States from ambient seismic noise: Rayleigh wave group velocity maps. Geochem. Geophys. Geosyst. 8 (8), Q08010.

Nicolson, H., Curtis, A., Baptie, B., Galetti, E., 2011. Seismic interferometry and ambient noise tomography in the British Isles. Proc. Geol. Assoc. http://dx.doi.org/10.1016/j.pgeola.2011.04.002.

Ramirez, A.C., Weglein, A.B., 2009. Green's theorem as a comprehensive framework for data reconstruction, regularization, wavefield separation, seismic interferometry, and wavelet estimation: a tutorial. Geophysics 74 (6), W35–W62, http://dx.doi.org/10.1190/1.3237118.

Reyners, M., Eberhart-Phillips, D., Stuart, G., Nishimura, Y., 2006. Imaging subduction from the trench to 300 km depth beneath the central North Island, New Zealand, with *Vp* and *Vp*/*Vs*. Geophys. J. Int. 165 (2), 565–583.

Rickett, J.E., Claerbout, J.F., 2000. Calculation of the acoustic solar impulse response by multi-dimensional spectral factorization. Solar Phys. 192, 203–210.

Ruigrok, E., Campman, X., Draganov, D., Wapenaar, K., 2010. High-resolution lithospheric imaging with seismic interferometry. Geophys. J. Int. 183, 339–357.

Sabra, K.G., Gerstoft, P., Roux, P., Kuperman, W.A., Fehler, M., 2005. Surface-wave tomography from microseisms in southern California. Geophys. Res. Lett. 32, L14311.

Sens-Schönfelder, C., 2008. Synchronizing seismic networks with ambient noise. Geophys. J. Int. 174, 966–970, http://dx.doi.org/10.1111/j.1365-246X.2008.03842.x.

Shapiro, N., Campillo, M., Stehly, L., Ritzwoller, M., 2005. High-resolution surface-wave tomography from ambient seismic noise. Science 307, 1615–1617.

Slob, E., Draganov, D., Wapenaar, K., 2007. Interferometric electromagnetic Green's functions representations using propagation invariants. Geophys. J. Int. 169, 60–80.

Slob, E., Wapenaar, K., 2007. Electromagnetic Green's functions retrieval by cross-correlation and cross-convolution in media with losses. Geophys. Res. Lett 34 (L05307-1–L05307-5).

Snieder, R., 2004. Extracting the Green's function from the correlation ofcoda waves: a derivation based on stationary phase. Phys. Rev. E 69, 046610.

Snieder, R., 2007. Extracting the Green's function of attenuating heterogeneous media from uncorrelated waves. J. Acoust. Soc. Am. 121, 2637–2643.

Snieder, R., van Wijk, K., Haney, M., Calvert, R., 2008. The cancellation of spurious arrivals in Green's function extraction and the generalised optical theorem. Phys. Rev. E 78, 036606.

Snieder, R., Wapenaar, K., Wegler, 2007. Unified Green's function retrieval by cross-correlation; connection with energy principles. Phys. Rev. E 75, 036103.

Stehly, L., Campillo, M., Froment, B., Weaver, R.L., 2008. Reconstructing green's function by correlation of the coda of the correlation (C3) of ambient seismic noise. J. Geophys. Res. 113, B11306. http://dx.doi.org/10.1029/2008JB005693.

Thorbecke, J., Wapenaar, K., 2007. On the relation between seismic interferometry and the migration resolution function. Geophysics 72, T61–T66.

van Manen, D.-J., Robertsson, J.O.A., Curtis, A., 2005. Modeling of wave propagation in inhomogeneous media. Phys. Rev. Lett. 94 (16), 164301-1–164301-4.

van Manen, D.-J., Curtis, A., Robertsson, J.O.A., 2006. Interferometric modelling of wave propagation in inhomogeneous elastic media using time-reversal and reciprocity. Geophysics 71 (4), SI47–SI60.

van Manen, D.-J., Robertsson, J.O.A., Curtis, A., 2007. Exact wavefield simulation for finite-volume scattering problems. J. Acoust. Soc. Am. Express. Lett. 122 (4), EL115–EL121, http://dx.doi.org/10.1121/1.2771371.

Vasconcelos, I., Sava, P., Douma, H., 2010. Nonlinear extended images via image-domain interferometry. Geophysics 75 (6), SA105–SA115, http://dx.doi.org/10.1190/1.3494083.

Wapenaar, K., 2004. Retrieving the elastodynamic Green's function of an arbitrary inhomogeneous medium by cross correlation. Phys. Rev. Lett. 93, 254301.

Wapenaar, K., 2006. Green's function retrieval by cross-correlation in case of one-sided illumination. Geophys. Res. Lett. 33 (L19304-1–L19304-6).

Wapenaar, K., Fokkema, J., 2006. Green's function representations for seismic interferometry. Geophysics 71 (4), SI33–SI44.

Wapenaar, K., Slob, E., Snieder, R., 2006. Unified Green's function retrieval by cross correlation. Phys. Rev. Lett. 97, 234301.

Wapenaar, K., Draganov, D., Snieder, R., Campman, X., Verdel, A., 2010a. Tutorial on seismic interferometry: part 1—basic principles and applications. Geophys 75 (75A195–75A209).

Wapenaar, K., Slob, E., Snieder, R., Curtis, A., 2010b. Tutorial on seismic interferometry: part 2—underlying theory and new advances. Geophysics 75 (75A211–75A227).

Weaver, R.L., Lobkis, O.I., 2001. Ultrasonics without a source: thermal fluctuation correlations at MHz frequencies. Phys. Rev. Lett. 87, 134301.

Yang, Y., Ritzwoller, M.H., Levshin, A.L., Shapiro, N.M., 2007. Ambient noise Rayleigh wave tomography across Europe. Geophys. J. Int. 168 (1), 259–274.